

Acute Rat Cutaneous Wound Healing for Small and Large Wounds Using Ar/O₂ Atmospheric-Pressure Plasma Jet Treatment

Zhi-Hua Lin,^a Kuang-Yao Cheng,^a Yu-Pin Cheng,^{b,c} Chen-Yon Tobias Tschang,^a Hsien-Yi Chiu,^d Nai-Lun Yeh,^e Kou-Chi Liao,^f Bi-Ren Gu,^a & Jong-Shinn Wu^{a,*}

^aDepartment of Mechanical Engineering, National Chiao Tung University, Hsinchu 300, Taiwan;

^bDepartment of Dermatology, Cathay General Hospital, Taipei 106, Taiwan; ^cDepartment of Biological Science and Technology, National Chiao Tung University, Hsin-Chu 300, Taiwan;

^dDepartment of Dermatology, National Taiwan University Hospital Hsinchu Branch, Hsinchu 300, Taiwan; ^eDepartment of Department of Family Medicine, National Taiwan University Hospital Hsinchu Branch, Hsinchu 300, Taiwan; ^fDepartment of Bio-industrial Mechatronics Engineering, National Taiwan University, Taipei 106, Taiwan

*Address all correspondence to: Jong-Shinn Wu, Department of Mechanical Engineering, National Chiao Tung University, 1001 Ta-Hsueh Road, Hsinchu 300, Taiwan; Tel.: 886-3-573-1693; Fax: 886-3-611-0023, E-mail: chongsin@faculty.nctu.edu.tw

ABSTRACT: In this study, we developed a rat model of acute wound healing treated by a cold and touchable Ar/O₂ atmospheric-pressure plasma jet (APPJ) with a jet gas temperature of < 37°C and a length of 15 mm. To generate more abundant reactive oxygen species (ROS) and reactive nitrogen species (RNS), we added various amounts of oxygen into argon. We have found that, with 0.04% oxygen addition, the APPJ can generate the most abundant ROS/RNS such as hydroxyl radicals (OH*), N₂^{2nd+}, and O atom in the jet region based on the optical emission spectroscopy measurements. We then applied the APPJ to treat open wounds of rats directly. To demonstrate the effectiveness of this APPJ treatment for wound healing, we created two wound sizes with diameters of 8 mm (small) and 21 mm (large). The results show that APPJ treatment with 0.04% oxygen addition can greatly accelerate wound healing, especially for the group with large wounds compared with the control group without any treatment. We explain this wound-healing enhancement with plasma jet treatment using a standard histologic method, hematoxylin and eosin staining, from the sectioned skins by comparing the different experimental groups.

KEY WORDS: atmospheric pressure plasma, dielectric barrier discharge, wound healing, animal model

I. INTRODUCTION

The skin is the largest organ of a human body and serves as a barrier to protect muscles, bones, and other organs from a potential threat from the environment. Damage of skin surface caused from injury or illness may lead to serious disability or even death.^{1,2} Most acute small wound healing can proceed without obstacles and only lasts for days to weeks without any proactive medical treatment. Therefore, accelerating the large acute wound-healing process to prevent infection is important in clinical practice. There are many traditional ways of treating acute wounds, including wound dressing and laser

and hyperbaric oxygen therapy.^{3–5} Recently, application of atmospheric-pressure plasma jet (APPJ) to speed up wound healing has become a promising alternative.^{6–9} However, these studies only treated small-size wounds of <10 mm in diameter. Therefore, the major objective of the current study was to apply an in-house argon APPJ to treat acute cutaneous wounds of varying sizes in the rat in order to understand its underlying mechanism using histology.

It is well known that the repair of cutaneous wound includes four phases: hemostasis, inflammation, proliferation, and tissue maturation. Hemostasis stops bleeding and activates the coagulation cascade when lesion is made. Inflammation recruits inflammatory cells such as neutrophils and macrophages to clean out damaged and dead cells, which eliminates pathogens from the environment. In this phase, the blood vessels expand to allow more oxygen and nutrient exchange to the wound. In addition, some growth factors are released into the wound that cause the migration and division of cells during the proliferation phase. In the proliferation phase, the fibroblasts synthesize extracellular matrix and collagen deposition to repair the breach, which plays an important role in supporting tissue structure. Angiogenesis, granulation tissue formation, epithelialization, and wound contraction occur in this stage. The final remodel (or tissue maturation) phase increases tissue tensile strength and mature scar tissue.^{6,10}

During wound healing, every stage is dynamic and different kinds of cells are involved. For instance, macrophages have been described to have many functions in the inflammation and proliferation phases, such as the promotion of inflammation, fibroblast proliferation support, and extracellular matrix synthesis. Macrophages are also unique in wound healing in that they remove neutrophils and apoptotic cell from wound sites.¹¹ The cell–cell interaction is complex and each cell has to communicate with each other in response to the change in environment. In fact, the cell signal requires reactive oxygen/nitrogen species (ROS/RNS) as a medium for delivery.¹² The role of ROS/RNS is important because they react relatively quickly to proteins, cells, tissues, and even biological fluid. In a typical wound-healing process, H₂O₂ has long been known for being the second messenger of tissue growth factor, platelet-derived growth factor, and vascular endothelial growth factor. It participates in blood coagulation and wound contraction.¹³ It is also an active species for bacteria inactivation through lipid peroxidation.^{14,15} NO is another key species in wound healing, having been proven to activate the function of angiogenesis, inflammation, and tissue remodeling to speed up recovery from cutaneous injury. In angiogenesis process, NO is able to stimulate endothelial cell proliferation and to prevent cell apoptosis. In other words, the new blood vessel formation in the wound site is promoted through the existence of NO.^{16,17} In our previous study, we found that trace amounts of oxygen addition into major discharge gas could enhance the relative emission intensity of ROS such as oxygen and OH. It can also result in significant improvement in inactivating either bacteria or endospores.¹⁸

Therefore, the objective of this study was to investigate the efficacy of applying an in-house APPJ using argon mixing with a trace amount of oxygen on acute wounds of rats. We measured the gas temperature and relative emission intensity in the jet region

of the APPJ using a thermometer and optical emission spectroscopy (OES). We applied the APPJ to treat two sizes of wounds on rats and compared the wound-healing speed with a control group without any treatment and with a traditional treatment group. The data were then analyzed and investigated using histology (through histological method (hematoxylin and eosin, H&E) of the skin tissues. Major findings of this study are summarized at the end.

II. MATERIALS AND METHODS

A. APPJ Facility and Instrumentation

Figure 1 shows the schematic diagram and image of the argon APPJ system with an in-house high-voltage compact power supply (0-20 kV peak-to-peak, 20-25 kHz, max. 60 W, 10 × 10 × 20 cm³). In addition to the powered and grounded electrodes, another floating electrode in direct contact with gas flow was added to enhance the plasma intensity. We have described the design details of the APPJ device previously.¹⁹ The working gas was argon (99.99%) with impurities (O₂ and H₂O in the order of 10 ppm for the former and a few ppm for the latter, respectively) at a flow rate of 5 slm. Oxygen was added when necessary and the flow rate was controlled by a mass flow controller. All images were captured by a digital camera with a prime lens. The electrical properties of the gas discharge were measured using a high-voltage probe (P6015A, Tektronix) and a Rogowski coil type current monitor with an output sensitivity of 1 volt/amp (IPC CM-100-MG, Ion Physics Corporation) through a digital oscilloscope (TDS1012B, Tektronix).

We observed the species of plasma jet in the post-discharge region using OES. The instrument was set with a 25 μm slit to meet 1 nm resolution (HR4000, Ocean Optics). A collimating lens (Model 74-UV) with a focal length of 10 mm, which could bring the collimated light to a diameter of 2 mm from the operating point of the APPJ, was fixed on the 2D moving stage for measuring OES data at various locations. Then, spectroscopy fitting software, PlausSpecLine, was used to analyze the measured spectra. We measured the plasma gas temperature continuously using a thermometer at a treating distance of 5 mm from the jet exit for both the free jet and jet-skin cases.

B. Animal Model Protocol

Sprague Dawley (SD) male rats aged 8 weeks and weighing 275-300 g (BioLASCO, Taiwan) were used.^{20,21} The rats were kept in the air-conditioned room at 22 ± 1°C and 55 ± 5% humidity with a 12 hour light/dark cycle, in accordance with the National Institutes of Health's *Guide for Care and Use of Laboratory Animals*.²² Each rat was caged individually to prevent biting and fighting during the wound-healing period. Water and standard laboratory chow were provided to the rats individually. In order to keep rats from pain and struggling during the initial wound creation surgery, they were anesthetized with 3% isoflurane inhalation. The tails were pressured and stimu-

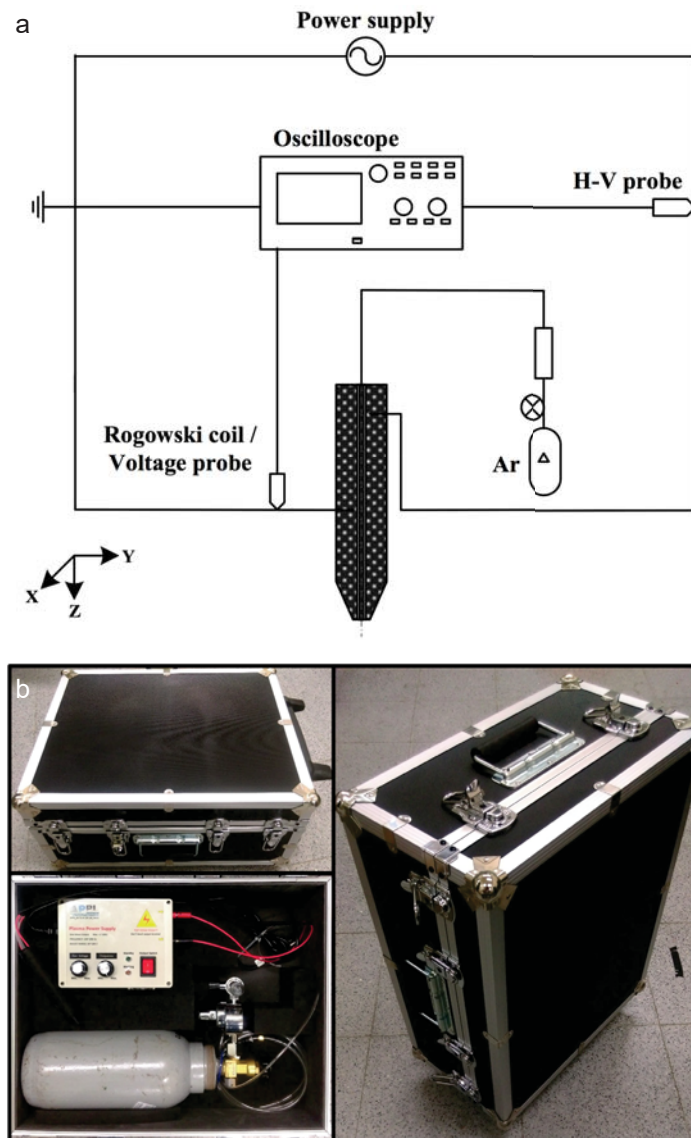


FIG. 1: (a) Schematic diagram of APPJ device with instrumentation. (b) Photo of a portable APPJ device

lated with forceps to ensure that they were completely unconscious. The hair on the rat's backs was shaved by an electric clipper before surgery. Two full-thickness round wounds were created on the both sides of dorsum with an 8 mm sterilized biopsy punch for the small wound and with clippers based on a 21 mm sterilized Taiwanese coin for the large wound. The rats were chosen randomly and subsequently divided into four groups: (1) the control group (CT), in which the wounds repaired spontane-

ously without any treatment; (2) the dressing (DS) group, in which the wounds were dressed, which is a commonly used wound-healing treatment; (3) the argon APPJ treatment group (PT); and (4) the argon APPJ treatment with 0.04% oxygen mixture group (PO). A total of 40 rats were used in this study, with 10 rats in each group. The small wounds in groups PT and PO were exposed to the direct APPJ treatment for 90 sec once per day after the wounds were created until they were healed at the end of the tests. For large wounds in groups PT and PO, we increased the plasma jet treatment time to 240 sec for a fair comparison between large and small wounds. We performed the jet treatment for the large wounds by slowly circling the wounds from outside to inside to make sure that all wounded areas were treated. We did not scale up the plasma jet treatment based on area mainly because the jet temperature would be too high, which may cause some damage to the epidermis. Indeed, more treatment strategies could be designed and applied; however, we did not explore them in the current study and they may be further investigated in the near future.

C. Wound-Healing Analysis

The day that wounds were created was defined as day 0. Observation of the wound kinetics could indicate the preliminary healing level. We imaged the wounds every day from day 0 until they were totally recovered. The wound areas were calculated by ImageJ image analysis software.²³ The wound area ratio was defined as follows: (current wound area/initial wound area) \times 100% to quantify the wound-healing speed for evaluating healing efficacy.

In the histology analysis, we used H&E staining, which is the standard method used to obtain tissue morphology. The wound tissues were removed from the skin with an 8 mm biopsy punch for the small wound. For the large wound, we used a Taiwanese coin with a diameter about 21 mm to draw a circle on the rat dorsal skin and cut the skin along the circle line using clippers. We followed the standard protocol²⁴ to prepare the slices in paraffin sections 3 μ m in thickness for H&E analysis. The histologic section images were acquired with a microscope (DM IL, Leica) with 40 \times magnification.

III. RESULTS AND DISCUSSION

A. APPJ Characterization

Figure 2 shows the typical measured waveform of applied voltage and average induced discharge current of the argon APPJ. The current generally leads the voltage slightly less than 90°, which is very similar to a typical capacitively coupled plasma. The applied voltage was 7.5 kV in amplitude and the maximal average currents were \sim 10 mA. There were generally four current spikes in each cycle. Even though the magnitudes of the first (positive) and third (negative) current peaks in each cycle vary one cycle from another cycle, their temporal positions are relatively invariant when the voltage is $\sim \pm 2.5$ –3 kV. We suspect that these narrow spikes (first and third) may be attributed to the use of float-

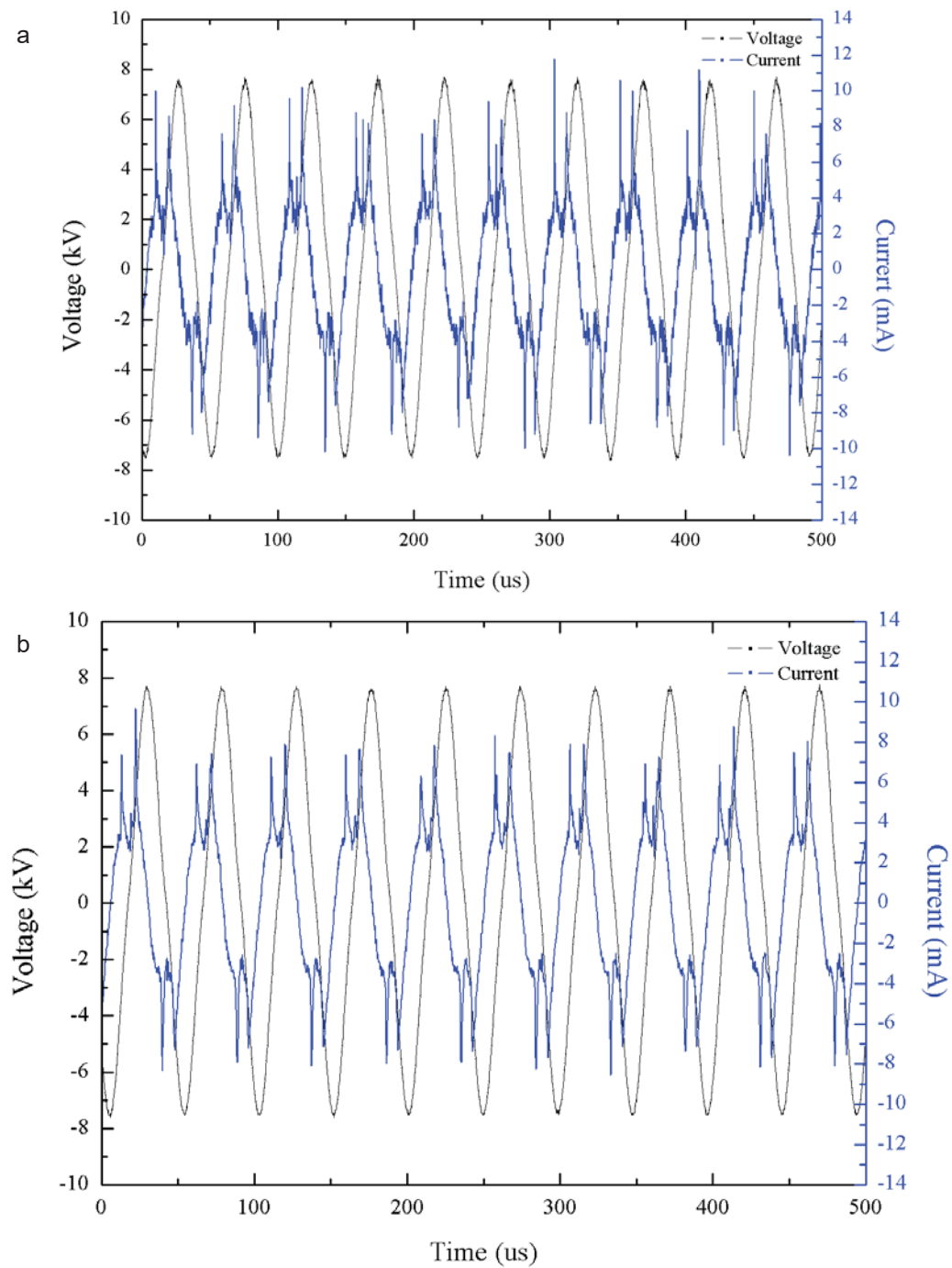


FIG. 2: Measured temporal current–voltage data of argon APPJ with typical operating conditions (V_{pp} : 15 kV, f : 20 kHz, argon: 5 slm). Shown are current data snapshot (a) and averaged for 64 measurements (b).

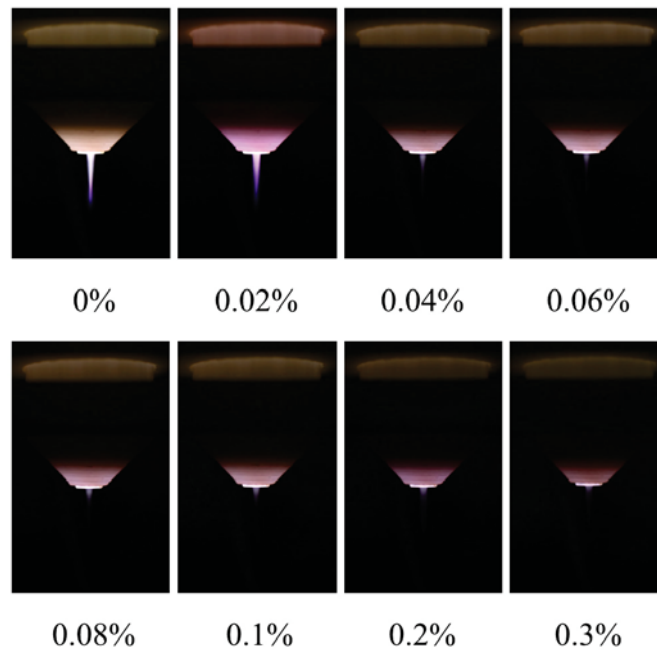


FIG. 3: Images of argon APPJ under operation with different levels of oxygen addition (exposure time: 1 sec)

ing electrode in the current APPJ design, in addition to the use of powered and ground electrodes. Further investigation into the cause of these two current spikes will be necessary because the calculated averaged power was found to be as low as ~ 2 W.

Figure 3 shows the images of argon APPJ with different levels of oxygen addition with an exposure time of 1 sec. The plasma jet plume becomes shorter and weaker with increasing amount of added oxygen because the oxygen molecules have very high electron affinity, which can reduce the number of electrons for plasma generation. Figure 4 shows a series of OES spectral data of argon APPJ measured at $x = 5$ mm in a free jet and at an interface where the plasma jet interacts with the intact skin ($x = 5$ mm) with different levels of oxygen added in the UV range (28–400 nm) and visible range (680–900 nm). The results indicate that the relative intensity of all ranges of measurement were enhanced several times (up to 4–5 times) compared with those of the free jet when the plasma jet interacted with the epidermis of rats. The results also show that the relative intensities of all emissions reach the highest level of all the excited species when the 0.04% oxygen was added. The N_2^{2nd+} (337, 357, and 380 nm) and O (777 nm) atoms, which were not detected in a free jet, were clearly identified near the region of the jet–epidermis interface. This means that some chemical reactions occurred when the plasma jet interacted with the rat epidermis. The epidermis may form a floating electrode with which the plasma jet with charged species comes to interact. The locally

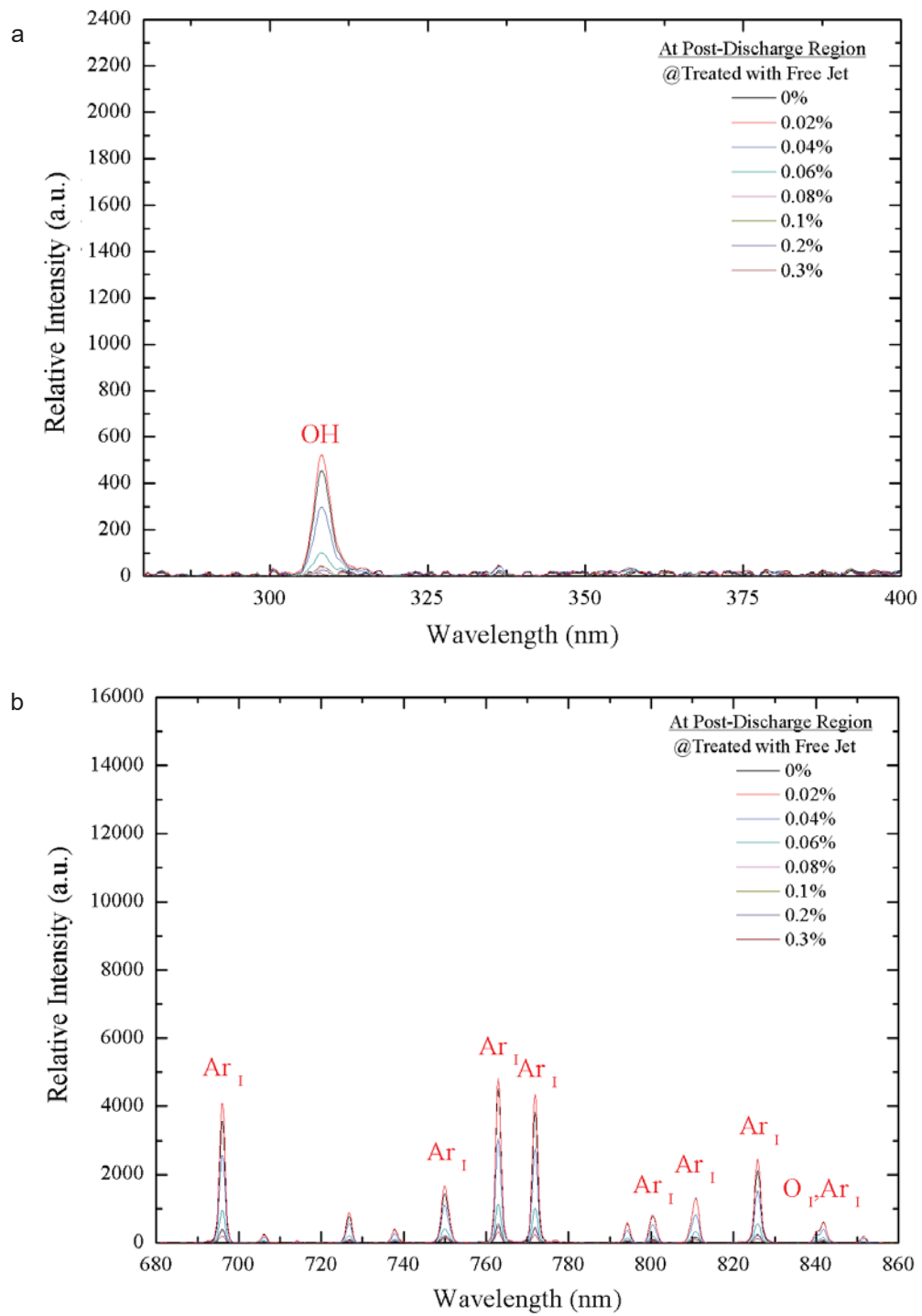


FIG. 4.

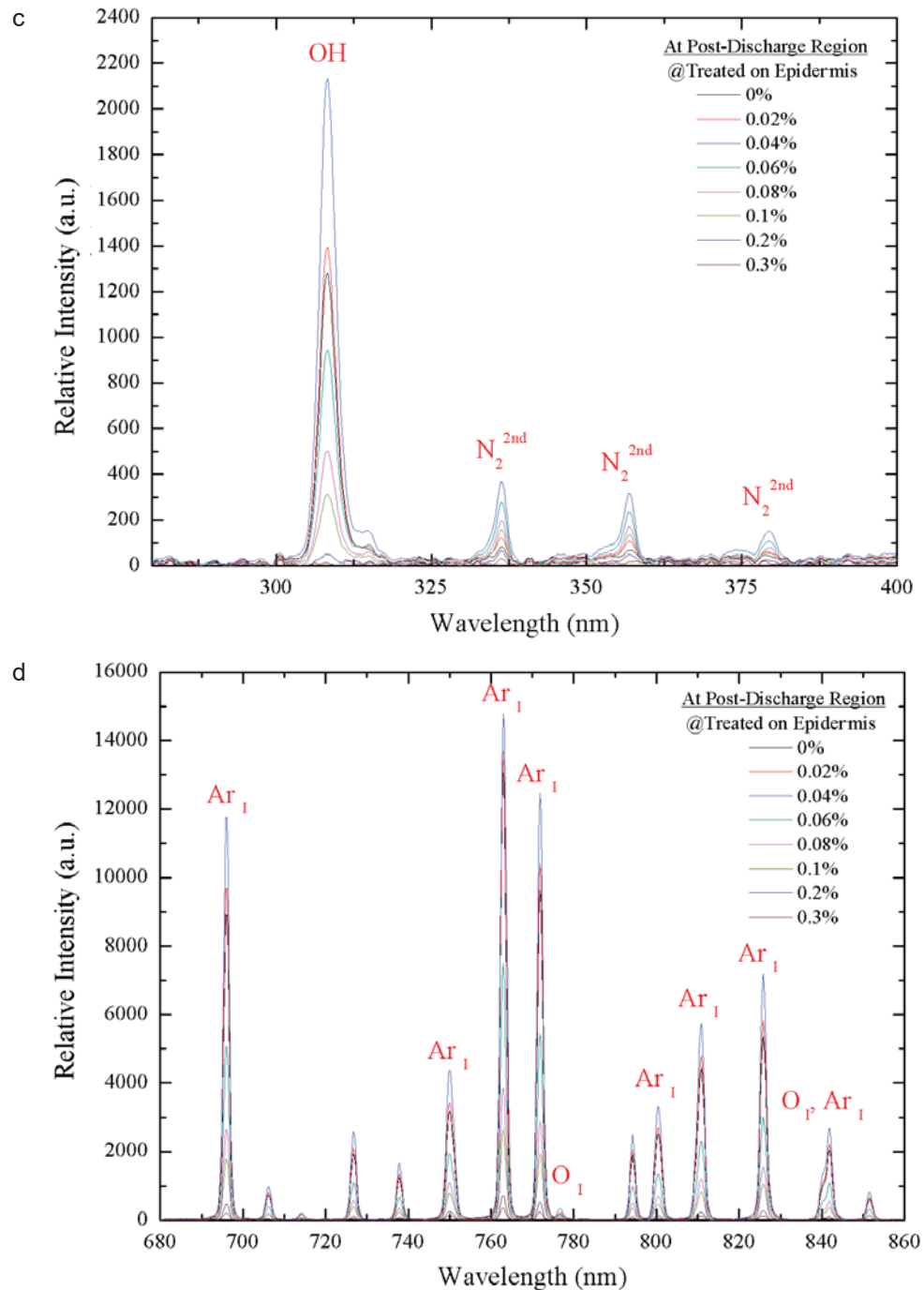


FIG. 4: OES spectra analysis of argon plasma with variant oxygen mixture. (a) Plasma treated on epidermis (280–400 nm). (b) Plasma free jet (280–400 nm). (c) Plasma treated on epidermis (680–900 nm). (d) Plasma free jet (680–900 nm).

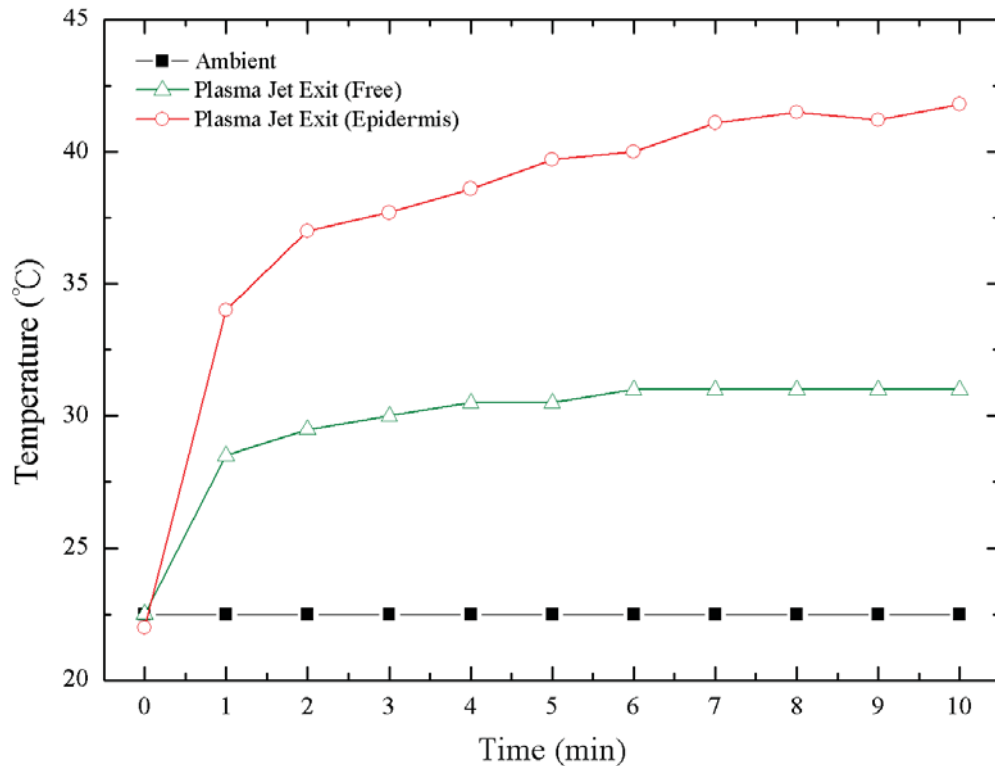


FIG. 5: Temporal gas temperature measurement in the post-discharge region of APPJ with various test conditions (V_{pp} : 15 kV, frequency: 20 kHz, argon: 5 slm)

enhanced electric field at the interface will increase the OES emission of many excited species, possibly originating from the gas source and ambient air with humidity.

B. Gas Temperature Measurement of APPJ

Touchable cold gas jet temperature is important in biomedical applications. Figure 5 shows the measured temporal gas temperature in the post-discharge region of the APPJ at $x = 5$ mm from the exit. The ambient temperature was $\sim 22^\circ\text{C}$ during the experiments. The results reveal that the gas temperature of the free jet is very cold, with a temperature of $\sim 31^\circ\text{C}$ for a continuous operation of 10 min. This means the plasma jet can be used for general biological tissue treatment without causing any thermal damage. In the case of the jet's interaction with rat epidermis, the gas temperature at the treatment location becomes close to 37°C after 4 min of operation, which is still very safe for most biomedical applications having direct contact with the human body. Even after 10 min of operation for the jet-skin interaction case, the temperature is only slightly above 40°C , which is acceptable for most biomedical applications.

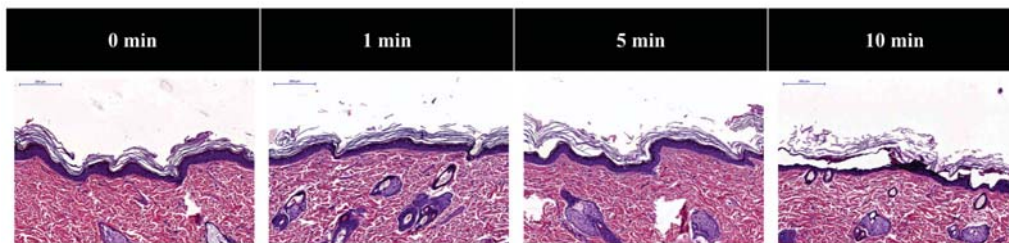


FIG. 6: H&E staining of the epidermis by continuous plasma jet treatment with different operating times

C. Safety Test of APPJ Treatment to Skin

To demonstrate that the APPJ does not do any harm to healthy skin, we used it to treat healthy epidermis for up to 10 continuous min and examined the skin using histological analysis. Figure 6 shows H&E staining for the tested epidermis with different plasma jet operating times with the control case. The results show that the epidermis and subcutaneous tissue with various operating times were essentially the same as that of healthy epidermis without any damage. Note that, after plasma jet treatment for 10 min, the epidermis becomes thicker than in the controls, so the argon plasma jet may cause slight damage to the stratum corneum. This further demonstrates that the proposed APPJ not only does not increase the temperature much, but also it does not cause any damage of the epidermis for operations lasting < 10 min.

D. Small Area Wound Healing

Figure 7 shows a series of typical visual images of small wound closure kinetics of the four experimental groups: control, dressing, argon plasma jet treatment with 0.04% oxygen addition, and pure argon plasma jet treatment. The dressings that we used were films from 3M (Model No. 1624W). Note that we performed 10 experiments for each group. The results show that group PO performed the best among all, especially up to day 7. However, after day 7 up to the end of the experiments (day 14), the difference was not obvious because of the very small wound area. Even the images in Fig. 7 show that the wounds of group PO seem to close totally on day 14. To be more specific, we quantified these observations using the wound-healing area ratio, as discussed below.

Figure 8 shows the evolution of small wound area ratios for different experimental groups during the wound-healing process. Note that we calculated the wound area ratio as defined above from 10 sets of visual images in each group using ImageJ software. We used an *ad hoc* preset threshold of the gray level for defining the wound boundary between wound and healthy areas, which would introduce some uncertainties of quantification. The initial idea wound area ratio (day 0) was set as 100%. On day 3, the wounds healed the fastest in group PO, as mentioned earlier, with a greatly reduced wound area

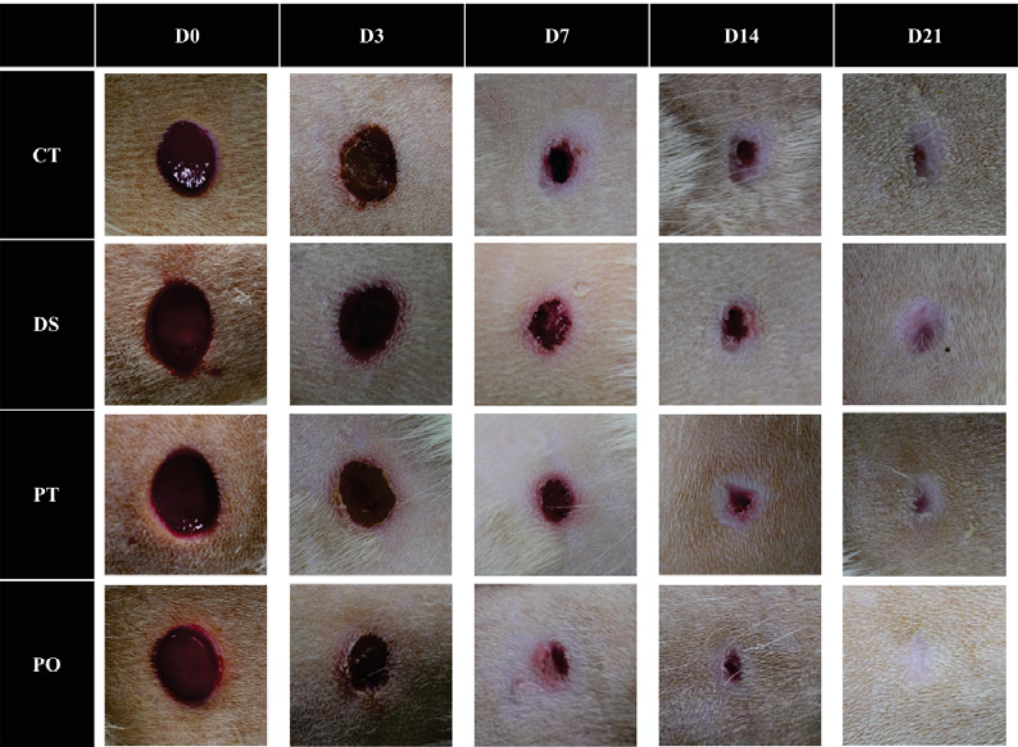


FIG. 7: Visual images of small wounds on various days during healing process for different APPJ treatment groups. CT, Control; DS, dressing; PT, argon plasma treatment; PO, argon plasma treatment with 0.04% O₂.

ratio up to 32% compared with group CT. In addition, the traditional dressing method was slower than group PO, with a larger wound area ratio of 18%. On day 7, the absolute reduction of wound area ratio of group PO compared with group CT and group DS was still appreciable (18% and 13%, respectively). After day 7, the wound area ratios became approximately the same within experimental uncertainties mainly because the areas were too small. In brief summary, the application of argon plasma jet with 0.04% oxygen addition to acute cutaneous wounds of rat skin did promote wound healing in the early stage up to day 7 within the experimental uncertainties.

Figure 9 shows the H&E staining of the four experimental groups as mentioned previously on different days (3, 7, 14, and 21) for small wounds. The figure shows the typical re-epithelialization process for all groups. On day 3, the wound surface was covered with scabs in all cases. However, we observed that the epithelial hyperplasia was more pronounced in the sample treated by plasma jet with 0.04% oxygen addition compared with the other groups. The keratinocytes proliferated, gradually migrated, and reached the wound surface below. The re-epithelialization process was taking place, notably extending to the wound surface. On day 7, the clear appearance of

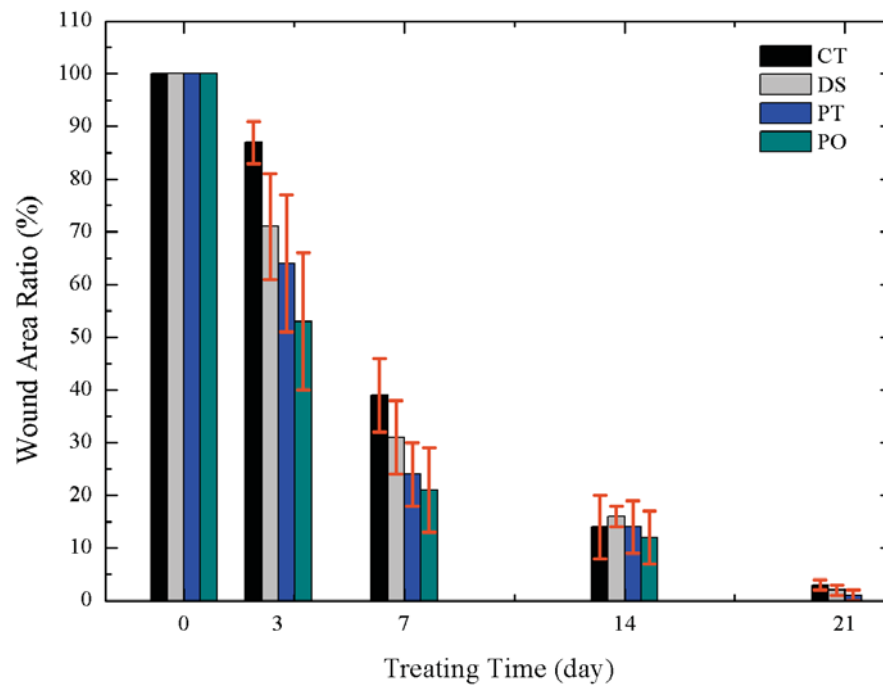


FIG. 8: Evolution of wound area ratio during the healing process for small wounds

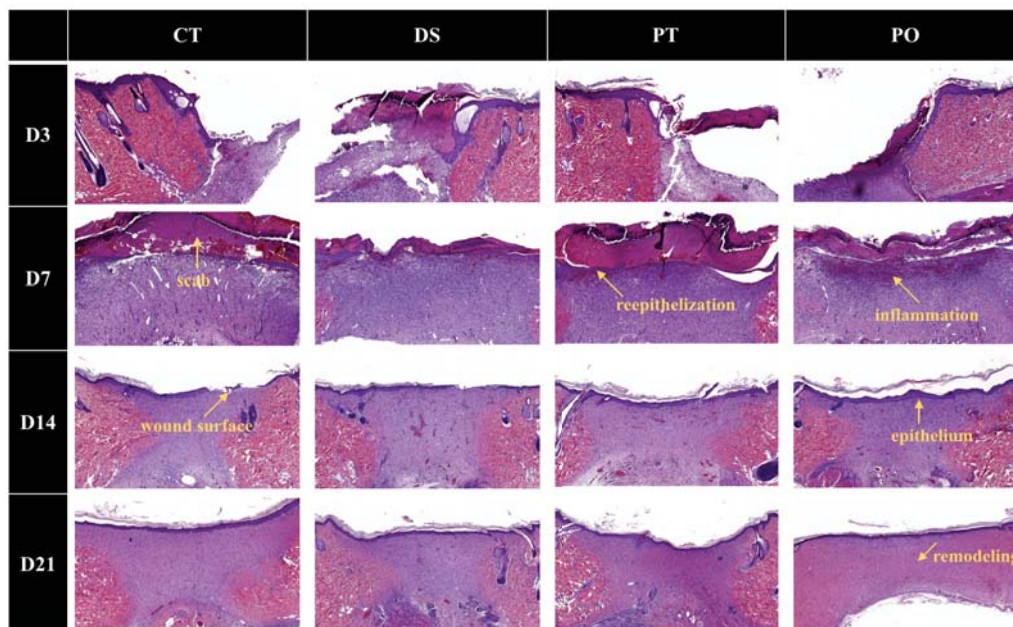


FIG. 9: H&E stain of control and argon plasma-treated tissues on days 3, 7, 14, and 21 for small wounds (all images are $\times 4$ magnification)

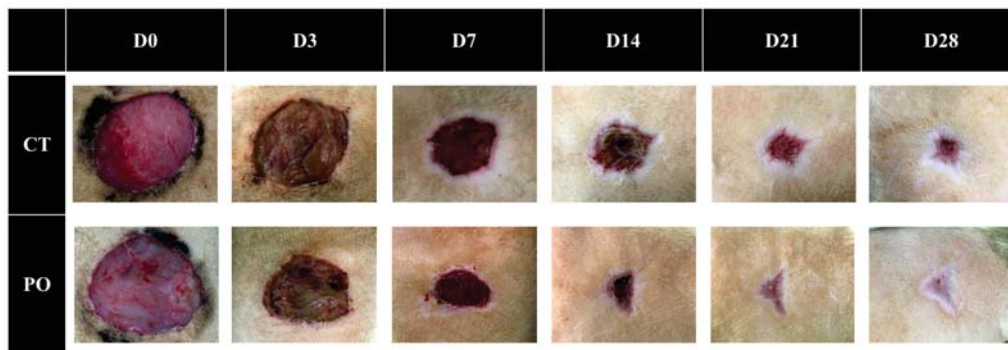


FIG. 10: Typical visual images of wounds on various days in the healing process of large wounds

inflammation developed near the wound border after plasma jet exposure, especially in the case of plasma jet with 0.04% oxygen addition. Most of the neutrophils and macrophages were found on the tissue surface. The CT and DS groups were still covered by scabs, which were shown to be eosinophilic after H&E staining and to be composed of necrotic cells. On day 14, the plasma jet-treated wounds were covered by continuous, alive epidermis and more abundant collagen formation, but those of the CT and DS groups were not. The granulation tissue formed progressively in plasma jet-treated cases and distinction of epidermis and dermis layer could be identified clearly. Finally, on day 21, all wounds were covered almost entirely by epidermis and almost completely healed. Interestingly, we have found that the cases with plasma jet-treated wounds had thicker epidermis, meaning that plasma-treated wounds, especially in plasma with 0.04% oxygen treatment, heal faster and better compared with other treatments.

E. Large Area Wound Healing

To further demonstrate the wound healing was not caused by the natural contraction of the rat's skin, we performed similar wound-healing experiments with larger wound areas with a diameter of ~21 mm. In this part of the study, we only wanted to compare the wound-healing process for large wounds with and without plasma treatment. Figure 10 shows a series of large area wound-healing images of group CT and group PO. The results clearly show the wound healing is greatly enhanced by the plasma jet treatment from the start to the end of the healing process compared with that of small wounds, as is further quantified in Fig. 11. As a result, the wound area with plasma treatment is much less than half of the CT group at the end of the test (day 28). With experimental uncertainties, we conclude that plasma jet treatment may be more effective in treating larger wounds than smaller wounds, but this conclusion requires further investigation.

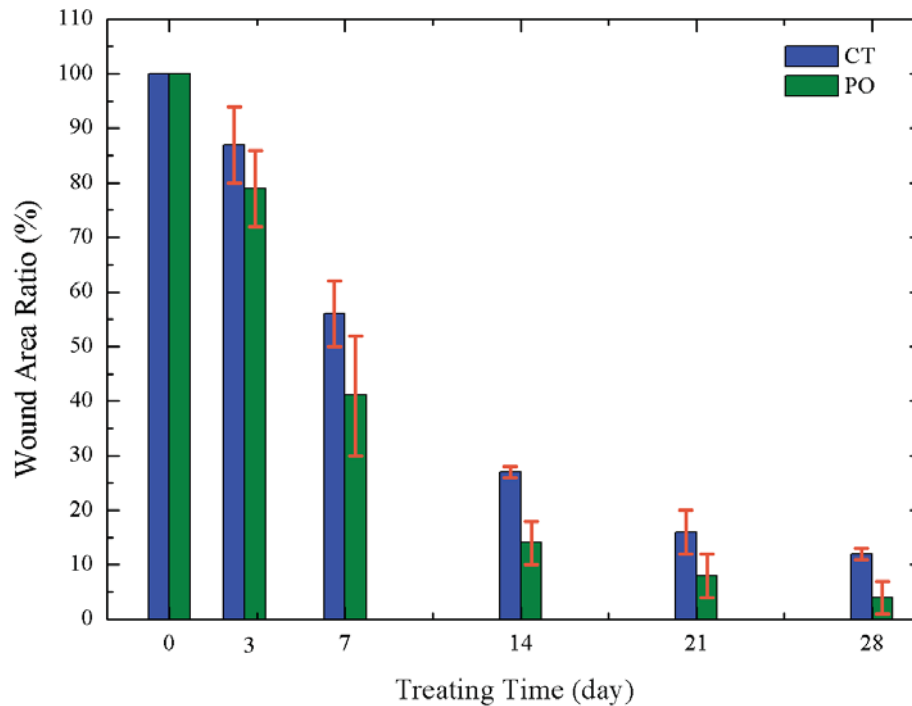


FIG. 11: Evolution of wound area ratio for large wounds

IV. CONCLUSION

In this study, we have successfully characterized an argon APPJ with 0.04% oxygen addition and investigated the efficacy of the wound-healing process by treating small and large acute cutaneous wounds directly on rat skin. The temperature measurements showed that the free jet is <37°C with <10 min of continuous operation, which is very safe for biomedical application. With APPJ interacting with the rat skin, the gas temperature near the skin is below 37°C within 4 min of operation. In addition, the plasma jet–skin interaction cases show 4–5 times enhancement of OES intensity (OH*), especially the cases with 0.04% oxygen addition, compared with the free jet cases. Interestingly, the N₂^{2nd+} and O atoms appeared in the former cases, but were not detected in the latter cases. H&E staining results indicate that the plasma jet treatment does not cause any thermal damage to healthy epidermis and subcutaneous tissues after continuous plasma jet treatment of <10 min. We have shown the wound-healing process for typical cases using H&E staining results. The results show that the wounds healed the fastest by using the APPJ with 0.4% of oxygen addition compared with the other test groups. This trend of wound healing is especially pronounced for the large wounds, for which the concern about natural contraction of rat skin could be disregarded. Studies on the underlying mechanism of the acute wound-healing process by plasma jet treatment are currently in

progress and will be reported in the near future.

ACKNOWLEDGMENTS

This work was supported by the Ministry of Science and Technology of Taiwan (Grant MOST-104-2221-E-009-150-MY3) and National Chiao Tung University (Grant HCH104-015). The authors thank Dr. Shiu-Feng Huang of the Pathology Core Laboratory of the National Health Research Research Institutes, Taiwan, for helpful discussion during the research.

REFERENCES

1. Baum C, Arpey C. Normal cutaneous wound healing: clinical correlation with cellular and molecular events. *Dermatol Surg*. 2005;31(6):674–86.
2. Epstein F, Singer A, Clark R. Cutaneous wound healing. *N Engl J Med*. 1999;341(10):738–46.
3. Mayet N, Choonara Y, Kumar P, Tomar L, Tyagi C, DuToit L, Pillay V. A comprehensive review of advanced biopolymeric wound healing systems. *J Pharm Sci*. 2014;103(8):2211–30.
4. Posten W, Wrone D, Dover J, Arndt K, Silapunt S, Alam M. Low-level laser therapy for wound healing: mechanism and efficacy. *Dermatol Surg*. 2006;31(3):334–40.
5. Gill A, Bell C. Hyperbaric oxygen: its uses, mechanisms of action and outcomes. *QJM*. 2004;97(7):385–95.
6. Kramer A, Lindequist U, Weltmann KD, Wilke C, Von Woedtke T. Plasma medicine: its perspective for wound therapy. *GMS Krankenhhyg Interdiszip*. 2008;3(1):Doc16.
7. Lloyd G, Friedman G, Jafri S, Schultz G, Fridman A, Harding K. Gas plasma: medical uses and developments in wound care. *Plasma Process Polym*. 2010;7(3–4):194–211.
8. Fridman G, Friedman G, Gutsol A, Shekhter AB, Vasilets VN, Fridman A. Applied plasma medicine. *Plasma Process Polym*. 2008;5(6):503–33.
9. Haertel B, Von Woedtke T, Weltmann KD, Lindequist U. Non-thermal atmospheric-pressure plasma possible application in wound healing. *Biomol Ther (Seoul)*. 2014;22(6):477–90.
10. Martin P. Wound healing: aiming for perfect skin regeneration. *Science*. 1997;276(5309):75–81.
11. Koh TJ, DiPietro LA. Inflammation and wound healing: the role of the macrophage. *Expert Rev Mol Med*. 2011;13:e23.
12. Graves DB. The emerging role of reactive oxygen and nitrogen species in redox biology and some implications for plasma applications to medicine and biology. *J Phys D Appl Phys*. 2012;45(26):263001.
13. Dunnill C, Patton T, Brennan J, Barrett J, Dryden M, Cooke J, Leaper D, Georgopoulos NT. Reactive oxygen species (ROS) and wound healing: functional role of ROS and emerging ROS-modulating technologies for augmentation of the healing process: Reactive oxygen species and wound healing. *Int Wound J*. 2017;14(1):89–96.
14. Golkowski M, Golkowski C, Leszczynski J, Plimpton SR, Maslowski P, Foltynowicz A, Foltynowicz R, Ye J, McCollister B. Hydrogen-peroxide-enhanced nonthermal plasma effluent for biomedical applications. *IEEE Trans Plasma Sci*. 2012;40(8):1984–91.
15. Joshi SG1, Cooper M, Yost A, Paff M, Ercan UK, Fridman G, Friedman G, Fridman A, Brooks AD. Non-thermal dielectric-barrier discharge plasma-induced inactivation involves oxidative DNA damage and membrane lipid peroxidation in *Escherichia coli*. *Antimicrob Agents Chemother*. 2011;55(3):1053–62.
16. Witte MB, Barbul A. Role of nitric oxide in wound repair. *Am J Surg*. 2002;183(4):406–12.
17. Luo JD, Chen AF. Nitric oxide: A newly discovered function on wound healing. *Acta Pharmacol Sin*. 2005;26(3):259–64.
18. Lin ZH, Tschang CY, Liao KC, Su CF, Wu JS, Ho MT. Ar/O argon-based round atmospheric-pressure

- plasma jet on sterilizing bacteria and endospores. *IEEE Trans Plasma Sci.* 2016;44(12):3140–7.
19. Lin ZH, Wu JS, Tschang CY, Su CF, Wu T, Shen YN, Liu CT, Jang WY, Ho MT. Development and characterization of a portable atmospheric-pressure argon plasma jet for sterilization. *IMECE* 2015. 2015;3:p. V003T03A075.
 20. Dunn L, Prosser H, Tan J, Vanags L, Ng M, Bursill C. Murine model of wound healing. *J Vis Exp.* 2013;(75):e50265.
 21. Dorsett Martin WA. Rat models of skin wound healing: A review. *Wound Repair Regen.* 2004;12(6):591–9.
 22. National Research Council of the National Academies. *Guide for the care and use of laboratory animals*, 8th ed. Washington, DC: National Academies Press; 2011.
 23. Wong VW1, Rustad KC, Galvez MG, Neofytou E, Glotzbach JP, Januszyk M, Major MR, Sorkin M, Longaker MT, Rajadas J, Gurtner GC. Engineered pullulan-collagen composite dermal hydrogels improve early cutaneous wound healing. *Tissue Eng Part A.* 2011;17(5–6):631–44.
 24. Fischer AH, Jacobson KA, Rose J, Zeller R. Hematoxylin and eosin staining of tissue and cell sections. *CSH Protoc.* 2008;2008:pdb.prot 4986.

